ACS APPLIED MATERIALS & INTERFACES

RESEARCH ARTICLE

www.acsami.org

Attachment of CdSe Nanoparticles to TiO_2 via Aqueous Linker-Assisted Assembly: Influence of Molecular Linkers on Electronic Properties and Interfacial Electron Transfer

Jeremy S. Nevins, Kathleen M. Coughlin, and David F. Watson*

Department of Chemistry, University at Buffalo, The State University of New York, Buffalo, New York 14260-3000, United States

Supporting Information

ABSTRACT: CdSe nanoparticles (NPs) capped with cysteinate (Cys), 3-mercaptopropionate (MP), and mercaptosuccinate (MS) were adsorbed to TiO_2 from basic aqueous dispersions. Native capping groups served as molecular linkers to TiO_2. Thus, the materials-assembly chemistry was simplified and made more reproducible and environmentally benign. The electronic properties of CdSe and the electron-transfer reactivity at CdSe-linker-TiO_2 interfaces varied with the structure and functionality of the capping groups. Cys-capped CdSe NPs exhibited a narrow and intense first excitonic absorption band centered at 422 nm, suggesting that they were magic-sized nanocrystals (MSCs) with diameters less than 2 nm. MP- and MS-capped CdSe NPs had broader and lower-energy absorption bands, which are typical of regular quantum dots. Photocurrent action spectra of nanocrystalline TiO_2 films functionalized with Cys-CdSe, MP-CdSe, and MS-CdSe overlaid closely with absorption spectra, indicating that excitation of CdSe gave rise to the injection of electrons into TiO_2. Under white-light illumination, the global energy-conversion efficiency for Cys-capped CdSe ($(0.45 \pm 0.11)\%$) was 1.2-to-6-fold greater than for MP- and MS-capped CdSe. Similarly, the absorbed photon-to-current efficiency was 1.3-to-3.3-fold greater. These differences arose from linker-dependent variations of electron-injection and charge-recombination reactivity. Transient absorption measurements indicated that electron injection from Cys-capped CdSe was more efficient than from MS-capped CdSe. In addition, charge recombination at CdSe-MS-TiO_2 interfaces was complete within hundreds of nanoseconds, whereas the charge-separated-state lifetime at CdSe-Cys-TiO_2 interfaces was on the order of several microseconds. Thus, Cys-capped CdSe MSCs are readily attached to TiO_2 and exhibit unusual electronic properties and desirable electron-transfer reactivity.

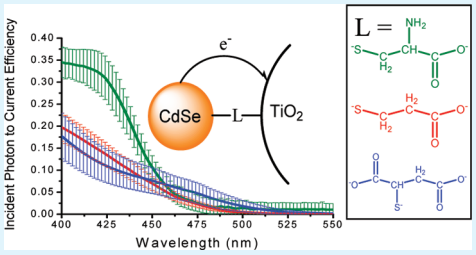

KEYWORDS: quantum dot solar cell, linker-assisted assembly, interfacial electron transfer, electron injection, charge recombination

INTRODUCTION

Semiconductor quantum dots (QDs) are intriguing alternatives to molecular chromophores and bulk semiconductors for light harvesting and solar energy conversion. QDs have size-dependent bandgaps, large oscillator strengths, and high cross sections for multiphoton absorption.[1−3] The phonon bottleneck may enable the extraction of nonthermalized charge carriers from photoexcited QDs,[4] and multiexciton generation can yield multiple electron−hole pairs following the absorption of a single photon under certain conditions.[5−10] Thus, QD-based photovoltaic devices and photocatalysts have the potential to exceed the Schockley-Queisser limiting efficiency.[4,11−13]

The QD-sensitized solar cell (QDSSC) is a promising approach.[11,13,14] Photoanodes of QDSSCs typically consist of nanostructured TiO_2 or ZnO films functionalized with II−VI or III−V QDs. The charge-separation mechanism is analogous to that of molecular dye-sensitized solar cells (DSSCs) and involves interfacial electron transfer, or electron injection, from photoexcited QDs into the conduction band or other acceptor states of the metal oxide. Two approaches have been explored for the in situ synthesis of QDs on metal oxide substrates: chemical bath deposition (CBD), in which substrates are immersed into mixed solutions of ionic precursors of QDs,[15] and successive ionic layer adsorption and reaction (SILAR), in which substrates are immersed sequentially into precursor solutions.[16,17] An alternative is to attach previously synthesized QDs to substrates by direct attachment (physisorption)[18−20] or by linker-assisted assembly, in which bifunctional molecules tether QDs to substrates.[21−24] To date, higher power conversion efficiencies have been realized for QDSSCs prepared by CBD and SILAR;[17,25,26] however, linker-assisted and direct attachment may afford greater control over the size and electronic properties of adsorbed QDs.[3,27−29] In addition, because linker-assisted assembly enables control over the distance and electronic coupling between QDs and substrates, it has been utilized for fundamental studies of interfacial electron-transfer reactions.[21,22,27−38]

Mercaptoalkanoic acids, mercaptobenzoic acids, and related linkers have been used to tether QDs to metal oxides by linker-assisted assembly.[21] Two approaches, herein referred to as methods 1 and 2, have been explored. Method 1 involves

Received: July 8, 2011
Accepted: October 4, 2011
Published: October 04, 2011

Chart 1. Structures of Bifunctional Ligands Used As Native Capping Groups and Linkers

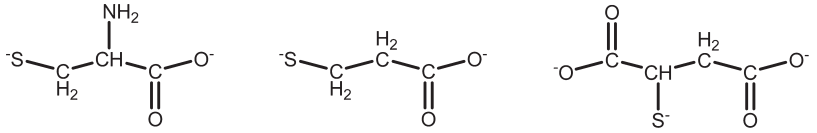

functionalization of a metal oxide with linkers followed by attachment of QDs to terminal functional groups of the adsorbed linkers.[20,22−24,27−29,39−42] In method 2, QDs are functionalized with linkers then attached to bare metal-oxide surfaces.[3,36,43−48] Method 1 assembly has received more attention; however, it often yields low and irreproducible surface coverages of QDs, particularly on porous nanostructured substrates.[3,20,41] Assembly via method 2 has been achieved either by displacing organic capping groups with bifunctional linkers or by using bifunctional linkers as native capping groups during the synthesis of QDs. Both approaches were recently shown to yield increased surface loadings of QDs on single-crystal TiO_2 relative to method 1 assembly.[3,45] Thus, linker-assisted assembly via method 2 may be an attractive strategy for functionalizing metal oxides with QDs.

In this manuscript, we report an all-aqueous route for the functionalization of nanocrystalline TiO_2 films with CdSe nanoparticles (NPs) via method-2 linker-assisted assembly. Three capping groups were used: cysteinate (Cys), 3-mercaptopropionate (MP), and mercaptosuccinate (MS) (Chart 1). The carboxylate groups of these linkers engender aqueous dispersibility and affinity for TiO_2. We have characterized the influence of the structure, functionality, and surface-attachment mode of capping groups on the electronic and photophysical properties of CdSe NPs, the affinity of NPs for TiO_2, the electron-transfer reactivity of CdSe-TiO_2 interfaces, and the photoelectrochemical performance of QDSSCs. We report that the electronic properties of Cys-capped CdSe NPs differ significantly from those of MP- and MS-capped CdSe NPs. Vibrational spectra and pH-dependent absorption spectra indicate that these effects arise from coordination of the amine group of Cys to the surface of CdSe NPs. Furthermore, we report that Cys promotes increased electron-injection yields and slower charge recombination. Our comparison of the linkers was motivated by recent spectroscopic results, which provide compelling evidence that the structure and properties of molecular linkers can significantly influence electron-transfer reactivity and the performance of QDSSCs.[22,28−30,49] Notably, Mora-Seró et al. reported that electron-injection rates and incident photon-to-current efficiencies (IPCEs) of QDSSCs prepared via method-1 assembly were greater with cysteine as linker than 3-mercaptopropionic acid.[42,49] The aqueous method-2 assembly chemistry reported in this manuscript represents a streamlined and "green" approach, in which CdSe NPs are tethered to TiO_2 without exchanging ligands at surfaces of NPs.

EXPERIMENTAL SECTION

Experimental details pertaining to the acquisition of materials and supplies, the determination of extinction coefficients of CdSe NPs, and the acquisition of transmission electron micrographs, X-ray powder diffraction data, infrared spectra, UV/vis absorption spectra, and emission spectra are provided in Appendix S1 of the Supporting Information.

Synthesis of CdSe NPs. CdSe NPs capped with Cys, MP, and MS are herein referred to as "Cys-CdSe", "MP-CdSe", and "MS-CdSe", respectively. NPs were synthesized in diH_2O under sufficiently basic conditions that the carboxylic acids of capping groups were deprotonated. Cys-CdSe was synthesized by adaptation of the method reported by Park et al.[50,51] A solution of sodium selenosulfate was prepared by dissolving selenium powder (0.17 g, 2.0 mmol) and sodium sulfite (0.80 g, 6.0 mmol) in deionized water (diH_2O) (42 mL). The mixture was refluxed overnight. The cadmium precursor was an 18-mL solution of cysteine (160 mM) and cadmium sulfate octahydrate (42 mM in Cd^{2+}) in diH_2O. The pH of the solution was titrated to 12.5−13.0 with solid NaOH. The hot sodium selenosulfate solution (7.5 mL) was added to the cadmium precursor with stirring. Typical concentrations of cadmium, selenium, and Cys in the reaction mixture were 30, 15, and 113 mM, respectively. Reaction mixtures were diluted 7-fold to prepare samples for spectroscopic analysis and comparison of particle-growth kinetics; molar ratios of reactants were held constant. MP-CdSe and MS-CdSe were synthesized by a similar procedure, but typical concentrations of MP and MS were 88 and 80 mM, respectively. Higher concentrations of MP and MS led to flocculation of CdSe NPs within 24 h.

Synthesis and Surface Functionalization of Nanocrystalline TiO_2 and ZrO_2 Films. Nanocrystalline TiO_2 and ZrO_2 films on glass substrates, which were used for equilibrium binding experiments and transient absorption measurements, were prepared by hydrolysis of titanium(IV) tetraisopropoxide and zirconium(IV) tetraisopropoxide, as described previously.[23,52,53] TiO_2 films were $(4.1 \pm 0.9)\ \mu$m thick and consisted of anatase TiO_2 particles with average diameters of (36 ± 6) nm.[23] ZrO_2 films were approximately 3 μm thick and consisted of nanoparticles in roughly spherical aggregates with diameters of (35 ± 6) nm.[53] Substrates for photoelectrochemical measurements were prepared by first depositing a dense blocking layer of TiO_2, which was intended to suppress back electron transfer reactions, onto fluorine-doped tin oxide (FTO)-coated glass slides following the method of Tachibana et al.[54] A layer of nanocrystalline TiO_2 was deposited on top of the blocking layer. The ruthenium 535 (N3) dye[55] was adsorbed to TiO_2 films from ethanol. CdSe NPs were adsorbed to TiO_2 and ZrO_2 films from aqueous dispersions at pH 12.5−13.0. Amounts of CdSe NPs per projected surface area of TiO_2 films, herein referred to as "surface coverages" and abbreviated as Γ, were calculated from absorbances at the first excitonic maxima of NP-functionalized films. We assumed that extinction coefficients were unchanged upon attachment of NPs to TiO_2. This assumption is supported by the lack of spectral changes upon immobilization of the NPs on TiO_2, as described below. In equilibrium binding experiments, TiO_2 films were immersed for 16 h at room temperature in stock reaction mixtures and various dilutions thereof. Surface coverages of CdSe NPs decreased as reaction mixtures aged. The highest surface coverages of CdSe NPs were achieved by immersing TiO_2 films in stock reaction mixtures within 30−60 min of combining the reagents. Films were soaked for 4−16 h in the stock reaction mixtures.

Transient Absorption Spectroscopy. Transient absorbance (TA) data were acquired with excitation at 415 nm (6−8 ns, $(1.0 \pm 0.3\ mJ/cm^2)$, 10 Hz) using instrumentation described previously.[28] The diameter of the pump beam was ~1 cm. TA difference spectra were compiled from single-wavelength decay traces and were normalized by dividing measured absorbance differences (ΔA) by the ground-state absorbance (A) at the excitation wavelength (415 nm). Suspensions of NPs were flowed through a four-sided cuvette with path length of 1 cm; flow was driven by a peristaltic pump. NP-functionalized TiO_2 and ZrO_2

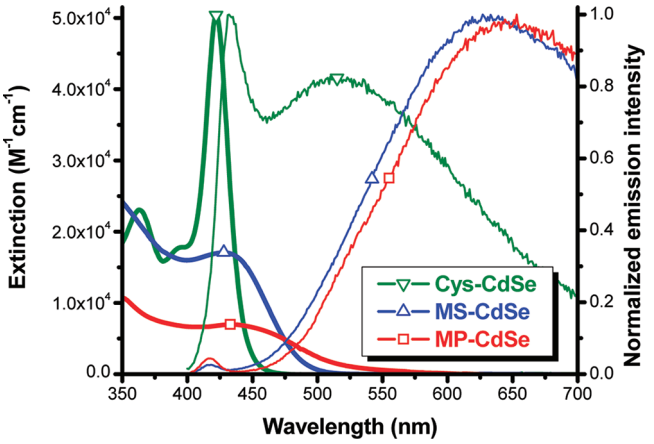

Figure 1. Absorption (thicker lines, left *y*-axis) and emission (thinner lines, right *y*-axis) spectra of as-synthesized reaction mixtures containing Cys-CdSe, MS-CdSe, and MP-CdSe at pH 12.5−13.0. Emission spectra were acquired with excitation at 365 nm.

films were immersed in Ar-saturated ethylene glycol within a four-sided cuvette with path length of 1 cm and were oriented at 45° to the pump and probe beams. To minimize photodegradation of adsorbed NPs, films were translated vertically during experiments such that different regions of the films were illuminated, and multiple films (9−22) were used during the acquisition of a given TA spectrum. All samples were purged with Ar for at least 10 min prior to data acquisition.

Photoelectrochemistry. Short-circuit photocurrent action spectra were acquired using instrumentation described previously.[56] N3 was used as a reference dye.[55] Two-electrode cells were assembled, consisting of a CdSe- or N3-functionalized TiO_2-on-FTO working electrode and either a PbS counter electrode (for QDSSCs) or a Pt-coated FTO counter electrode (for N3-sensitized cells). PbS electrodes were prepared following the method of Tachan et al.[57] Working and counter electrodes were separated by 12.7 mm within a Teflon cell containing 0.5 mL of electrolyte. An aqueous polysulfide electrolyte containing sodium sulfide (1 M), sulfur (0.1 M), and sodium hydroxide (0.1 M) was used for QDSSCs. For measurements on N3-coated TiO_2 films, the electrolyte consisted of iodine (0.05 M), lithium iodide (0.1 M), 1-methyl-3-propylimidazolium iodide (0.6 M), 4-*tert*-butylpyridine (0.6 M), and guanidinium isothiocyanate (0.1 M) in acetonitrile. The backside of the working electrode was illuminated with a 0.47 cm^2 beam. Monochromatic spectral irradiances ranged from 3.2×10^{-3} mW cm^{-2} nm^{-1} to 5.7×10^{-3} mW cm^{-2} nm^{-1}; the integrated irradiance was 1.2 mW cm^{-2}. The configuration of electrochemical cells was identical for photocurrent-photovoltage measurements. Data were acquired using the full output of a 75 W Xe lamp (Newport Photomax). The irradiance was 56 mW/cm^2. For each measurement, data were first acquired from short circuit to open circuit then from open circuit to short circuit.

RESULTS AND DISCUSSION

Photophysical Properties of CdSe NPs. Within 6−10 h after Cys-CdSe samples were flocculated from the reaction mixture and redispersed into basic water, the absorbance at the first excitonic maximum decreased by approximately 10% and a red-shifted band developed. The spectral changes continued over time, and solids flocculated after approximately one week. We recently reported on the chemistry associated with the degradation of Cys-CdSe.[58] In contrast, absorption spectra of MP-CdSe and MS-CdSe that had been flocculated then redispersed into water remained nearly superimposable with the spectra of as-synthesized reaction mixtures for at least one week. To avoid complications associated with the degradation of Cys-CdSe after removal from the original reaction mixture, we herein report absorption and emission spectra of as-synthesized reaction mixtures containing Cys-CdSe, MP-CdSe, or MS-CdSe. The reaction mixtures also contained free capping groups and unreacted cadmium and selenide precursors.

Absorption and emission spectra of CdSe-containing reaction mixtures are shown in Figure 1, and spectral parameters are compiled in Table 1. The absorption spectrum of Cys-CdSe was consistent with the spectrum reported by Park et al.[50,51] The first excitonic band was centered at 422 nm and had a full-width at half-maximum (fwhm) of 900 cm^{-1}. The spectrum contained a shoulder at 390 nm and a well-resolved band at 361 nm that probably corresponded to the second excitonic transition. The high energy and sharpness of the first excitonic band, as well as its large intensity relative to the second excitonic band, indicate the formation of CdSe NPs with diameters less than 2 nm.[59,60] The spectral features are consistent with those of monodisperse suspensions of thermodynamically stable magic-sized clusters (MSCs) of CdSe with diameters of 1.5−1.7 nm and containing 30−35 Cd ions.[50,61−69] Such MSCs may have core-cage crystal structures, rather than the typical wurtzite or zinc blende structures of CdSe QDs.[65] Our measured extinction coefficient at the first excitonic maximum of Cys-CdSe (5.0×10^4 M^{-1} cm^{-1}) was approximately twice the value calculated from the power function reported by Yu et al.[60] and was within 4−12% of the values reported by Soloviev et al. for CdSe MSCs containing 10−32 Cd^{2+} ions and dispersed in acetonitrile.[62] The emission spectrum of Cys-CdSe in a pH 13 aqueous dispersion consisted of a narrow band centered at 432 nm (fwhm ∼1100 cm^{-1}) and a broad band centered at approximately 515 nm (fwhm ∼6700 cm^{-1}). We attribute the higher-energy band to band-edge emission[70] and the lower-energy band to trap-state emission.[71−73] Our XRD data of Cys-CdSe NCs (see the Supporting Information, Figure S1) consisted of bands centered at 2θ values of 27° (fwhm of 6.8°) and 45° (fwhm of 7.7°). The peaks were significantly broader than those of bulk wurtzite or zinc-blende CdSe. Murray et al. reported similarly broad XRD features centered at 28° and 45° for 1.2-nm-diameter TOPO-capped CdSe NCs.[59] In summary, on the basis of their electronic spectra and XRD patterns, we conclude that as-synthesized Cys-CdSe NCs were MSCs with diameters less than 2 nm. Park and co-workers also suggested that the Cys-CdSe NCs prepared through their route were MSCs.[50,51]

The electronic spectra of MP-CdSe and MS-CdSe differed markedly from those of Cys-CdSe (Figure 1, Table 1). MP-CdSe and MS-CdSe exhibited red-shifted, broader, and less intense first excitonic transitions with maxima at approximately 433 and 428 nm, respectively. The second excitonic bands of MP-CdSe and MS-CdSe were more intense than the first. XRD data for MP-CdSe and MS-CdSe contained broad bands from ∼21 to 35° with wurtzite CdSe peaks at 23° (100), 25° (002), and 27° (101),[59] as well as broad bands from ∼40 to 50°. XRD data also contained peaks from ∼31 to 35°, which probably arose from the presence of cadmium oxide, cadmium hydroxide, and/or cadmium sulfate in the samples. The red-shifted and broadened absorption spectra and the XRD data of MP-CdSe and MS-CdSe are consistent with those of regular QDs with distributions of larger sizes,[59,74,75] rather than MSCs. Our measured extinction coefficients at the first excitonic maxima of MP-CdSe and MS-CdSe

Table 1. Selected Parameters from Absorption and Emission Spectra of CdSe NPs in Aqueous Dispersions at pH 12.5−13

	absorption			emission[a]		
sample	λ_{max} (nm) [b]	extinction coefficient at λ_{max} (M^{-1} cm^{-1})	fwhm [c] (cm^{-1})	$\lambda_{max,emis}$ (nm)	stokes shift [d] (cm^{-1})	fwhm (cm^{-1})
Cys-CdSe	422	50000	900	432 (BE [e])	550 (BE)	1100 (BE)
				515 (TS[f])	4300 (TS)	6700 (TS)
MP-CdSe	433	7000	2900	653 (TS)	8000 (TS)	5700 (TS)
MS-CdSe	428	17000	3400	627 (TS)	7400 (TS)	5900 (TS)

[a] With excitation at 365 nm. [b] λ_{max} = wavelength of first excitonic absorption maximum. [c] fwhm = full-width at half-maximum. [d] Relative to λ_{max}. [e] BE = band-edge. [f] TS = trap-state.

(Table 1) were, respectively, 7- and 3-fold lower than that of the first excitonic band of Cys-CdSe and 4- and 1.5-fold lower than values calculated using the power function of Yu et al.[60] The low extinction coefficients of MP-CdSe and MS-CdSe provide further evidence that as-synthesized dispersions contained regular CdSe QDs with distributions of sizes, in contrast to the Cys-CdSe MSCs or the nearly monodisperse CdSe NPs analyzed by Yu et al.[60] Emission spectra for MP-CdSe and MS-CdSe were slightly narrower and significantly red-shifted compared to the trap-state emission band of Cys-CdSe. Emission maxima for MP-CdSe and MS-CdSe were 653 and 627 nm, respectively. The large Stokes shifts (8000 and 7400 cm^{-1} for MP-CdSe and MS-CdSe, respectively) indicate that the bands arose exclusively from trap-state emission.

We attempted to characterize the sizes and size distributions of Cys-CdSe, MP-CdSe, and MS-CdSe samples using high-resolution transmission electron microscopy (TEM). However, the CdSe NPs coalesced and grew under the electron beam during spectral acquisition. Thus, we were unable to characterize accurately the sizes of as-synthesized NPs. Park et al. similarly reported that Cys-CdSe MSCs melted during high-resolution TEM experiments.[51]

Surface-Attachment Mode of Cys. The amine, carboxylate, and thiolate groups of fully deprotonated Cys are Lewis-basic and could potentially coordinate to Cd^{2+} sites at the surface of CdSe NPs. To evaluate the roles of these functional groups, we compared Fourier transform infrared (FTIR) spectra of zwitterionic free cysteine and Cys-CdSe NPs that had been flocculated from a pH 12.5 reaction mixture. Spectra are shown in Figure S2 in the Supporting Information, and peaks are assigned in Table S1 in Supporting Information. The FTIR spectrum of free cysteine was consistent with reported spectra.[76−78] The spectrum of Cys-CdSe exhibited broadened peaks and differed in several respects from the spectrum of free cysteine: (1) the stretching band of the thiol (ν(SH), 2552 cm^{-1})[76−78] and the asymmetric stretching band of the protonated amine ($\nu_a(NH_3^+)$, 3183 cm^{-1})[78] were absent; (2) the asymmetric and symmetric stretching bands of the carboxylate ($\nu_a(CO_2^-)$ and $\nu_s(CO_2^-)$, respectively)[76−78] were shifted, and a broad stretching band of neutral amine ($\nu(NH_2)$, ~3200−3500 cm^{-1})[76,79,80] was present. The thiol group of cysteine (pK_a 8.14)[81] was deprotonated in the pH 12.5 reaction mixture from which Cys-CdSe was isolated; thus, the ν(SH) band would be absent whether or not thiolate groups were coordinated to the surface of CdSe NPs. On the basis of reported structures of cadmium(II)-cysteinato complexes,[76−78,82] we assume that the thiolate of Cys was coordinated to Cd^{2+} surface sites. The amine of cysteine (pK_a 10.28)[81] was also deprotonated in the reaction mixture. The broad $\nu(NH_2)$ band in the spectrum of Cys-CdSe is similar to that of complexes and NPs bearing Cys coordinated through the amine.[51,76,79,83] Thus, we conclude that amines of CdSe-adsorbed Cys were predominantly coordinated to CdSe.

The frequency difference between $\nu_a(CO_2^-)$ and $\nu_s(CO_2^-)$ of carboxylates, designated as Δ, increases with decreasing symmetry of C−O bonds; therefore, Δ values of carboxylates coordinated to metals in monodentate geometry are greater than those of free carboxylates.[80,84,85] For amino acids, however, this trend is complicated by intramolecular H-bonding and H-bonding with water.[84] H-bonding lessens the asymmetry of monodentate-coordinated carboxylates. Values of Δ for H-bonded, monodentate-coordinated carboxylates are sometimes lower than those of free carboxylates.[80,84] The $\nu_a(CO_2^-)$ band in our FTIR spectrum of Cys-CdSe was broad, and its maximum (1575 cm^{-1}) was shifted to lower frequency than that of free cysteine (1590 cm^{-1}) (see the Supporting Information, Figure S2). The $\nu_s(CO_2^-)$ maximum of Cys-CdSe (1400 cm^{-1}) was shifted to higher frequency than $\nu_s(CO_2^-)$ of free cysteine (1394 cm^{-1}). Thus, the value of Δ for Cys-CdSe (175 cm^{-1}) was less than that of free cysteine (196 cm^{-1}). Similar values of Δ have been reported for cadmium(II) complexes bearing Cys or penicillamine ligands with coordinated carboxylates.[78,86] Therefore, our FTIR data imply that carboxylates of Cys were coordinated to surface Cd^{2+} sites of flocculated CdSe NPs. Cross-linking between NPs may have resulted in increased coordination of carboxylates in flocculated Cys-CdSe relative to dispersed Cys-CdSe. Furthermore, the $\nu_a(CO_2^-)$ band of Cys-CdSe was broader than that of free cysteine, and the $\nu_s(CO_2^-)$ band of Cys-CdSe had a well-resolved shoulder at 1386 cm^{-1}, which is lower than $\nu_s(CO_2^-)$ of free cysteine and gives rise to an increased value of Δ. Therefore, carboxylate groups of some of the Cys ions were evidently not coordinated to CdSe. The presence of some free carboxylates on CdSe is supported by the affinity of Cys-CdSe for TiO_2, as described below. In summary, Cys probably adsorbed to CdSe NPs in multiple geometries. We assume that thiolates were coordinated to Cd^{2+}, and our FTIR data indicate that amines and a fraction of carboxylates were coordinated to CdSe MSCs within flocculated solids.

Influence of the Amine of Cys on the Electronic Properties of CdSe. To explore further the influence of the coordinated amine group of Cys, we monitored the evolution of electronic spectra of Cys-CdSe NPs synthesized in dilute reaction mixtures at pH values of 9.5 and 13.0. The CdSe NPs grew slowly in the diluted reaction mixtures, allowing us to monitor kinetics in real time using UV/vis absorption spectroscopy. The pK_a of the amine of Cys is 10.28;[81] therefore, amines of approximately 85% of Cys ions were protonated at pH 9.5, whereas amines of only 0.2% of Cys ions were protonated at pH 13.0. (At pH values of 9.5 and 13.0, both the thiol (pK_a 8.14)[81] and carboxylic acid (pK_a 1.91)[81]

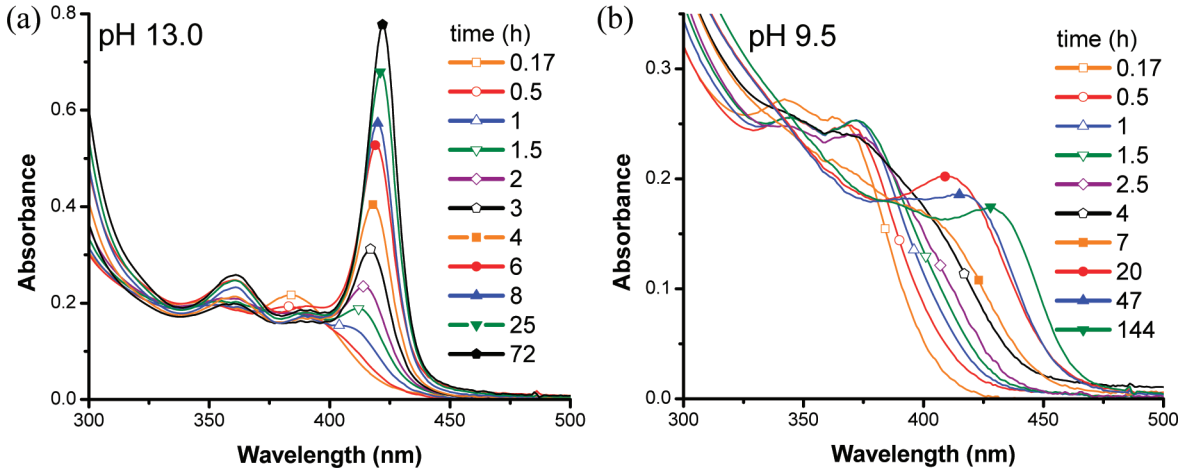

Figure 2. Absorption spectra of dilute Cys-CdSe reaction mixtures at (a) pH 13.0 and (b) pH 9.5 as a function of time after mixing aqueous solutions of sodium selenosulfate and the cadmium precursor.

were deprotonated in nearly all Cys ions.) For diluted reaction mixtures at pH 13.0, absorption spectra initially exhibited a broad band centered at approximately 385 nm (Figure 2a). A well-resolved and narrow first excitonic band developed within 1.5 h. This band red-shifted gradually, and its maximum remained constant at 422 nm after approximately 24 h. The particle-growth kinetics and spectral evolution were similar to those reported by Park et al.[68] Absorption spectra of pH-9.5 reaction mixtures evolved quite differently (Figure 2b). Spectra initially exhibited two overlapping bands with maxima of approximately 340 and 370 nm. The bands separated with reaction time, and the maximum of the lower-energy band, presumably the first excitonic band of CdSe, shifted to 428 nm after six days. The first excitonic band was red-shifted and much broader (fwhm ~2300 cm^{-1}) than that of Cys-CdSe MSCs synthesized at pH 13.0. Therefore, protonation of the amine of Cys resulted in the formation of regular CdSe QDs rather than MSCs.

Emission spectra of Cys-CdSe NPs synthesized at pH 9.5 (see the Supporting Information, Figure S3b) consisted only of a broad trap-state emission band centered at approximately 570 nm, at significantly lower energy than trap-state emission from Cys-CdSe MSCs synthesized at pH 13.0 (see the Supporting Information, Figure S3a). Band-edge emission was quenched completely at pH 9.5. Amine-bearing capping groups are known to promote enhanced band-edge emission and blue-shifted and intensified trap-state emission from cadmium chalcogenide QDs.[87−91] The effects have been attributed to the filling of electron-trap states and the shifting of electron-trap states to higher energies upon coordination of amines to surface Cd^{2+} sites.[87,88,90] Taken together, the narrower and blue-shifted first excitonic absorption band, the enhanced band-edge emission, and the blue-shifted trap-state emission of Cys-CdSe at pH 13.0, compared to pH 9.5, provide strong evidence that (1) the deprotonated amine group of Cys was coordinated to the surface of Cys-CdSe MSCs at pH 13.0 and (2) the amine group promotes the formation of MSCs. These conclusions are consistent with recent reports by our group and by Park et al.,[58,68] which suggested that $[Cd(Cys)_3]^{4-}$, a coordination complex with one bidentate Cys ligand in which the amine is coordinated to Cd^{2+},[92] is the precursor to Cys-CdSe MSCs.

Attachment of CdSe NPs to TiO_2. Immersion of NC TiO_2 films into aqueous dispersions of Cys-CdSe, MP-CdSe, or MS-CdSe caused the films to turn yellow due to attachment of CdSe NPs. Absorption spectra of wet CdSe-functionalized TiO_2 films, obtained immediately after removal from the reaction mixture and rinsing with diH_2O, were perturbed minimally relative to spectra of dispersed CdSe NPs (Figure 3). Cys-CdSe-modified TiO_2 films exhibited a well-resolved first excitonic transition centered at 422 nm (Figure 3a); the band maximum and fwhm were unchanged relative to dispersed Cys-CdSe. The first excitonic transitions of TiO_2-adsorbed MP-CdSe and MS-CdSe (Figure 3b, c) were blue-shifted by 10−15 nm (550−825 cm^{-1}) relative to the corresponding dispersed QDs. The high-energy sides of the bands overlapped with the onset of the bandgap transition of TiO_2. Alkanoic acids and carboxylated molecular dyes usually adsorb to TiO_2 by coordination of carboxylate oxygens to surface Ti^{4+} sites.[23,93−96] We assume that Cys-CdSe, MP-CdSe, and MS-CdSe attached to TiO_2 through the carboxylates of the capping agents.

Equilibrium binding experiments revealed the relative affinities of Cys-CdSe, MP-CdSe, and MS-CdSe for TiO_2 (Figure 4). Cys-CdSe and MS-CdSe did not appear to reach saturation surface coverages within the range of concentrations evaluated, whereas MP-CdSe may have. The highest measured surface coverages ranged from $(2.3 \pm 0.3) \times 10^{-8}$ mol cm^{-2} for MP-CdSe to $(3.5 \pm 0.5) \times 10^{-8}$ mol cm^{-2} for Cys-CdSe. These values are three-to-10-fold lower than typical surface coverages of molecular adsorbates on nanocrystalline TiO_2 films.[24,97−100] The decreased surface coverages of CdSe NPs are consistent with their increased size and footprint on the surface. Plots of surface coverage vs concentration were steeper for Cys-CdSe and MS-CdSe than for MP-CdSe. For TiO_2 films immersed in dispersions of CdSe NPs with a given concentration, the surface coverages of CdSe NPs were as follows: $\Gamma_{Cys\text{-}CdSe} > \Gamma_{MS\text{-}CdSe} > \Gamma_{MP\text{-}CdSe}$. The surface adduct formation constants (K_{ad}) probably decreased in the same order, but any differences in K_{ad} were minimal. Our data did not follow the Langmuir adsorption isotherm, and we did not attempt to estimate K_{ad} values. The increased affinity of MS-CdSe relative to MP-CdSe may have arisen from the presence of a second carboxylate group. Coordination of multiple carboxylate groups has been shown to increase the stability of molecular adsorbates on TiO_2.[24,95,100]

The origin of the higher measured surface coverages of Cys-CdSe is not obvious. Ataman et al. characterized the adsorption

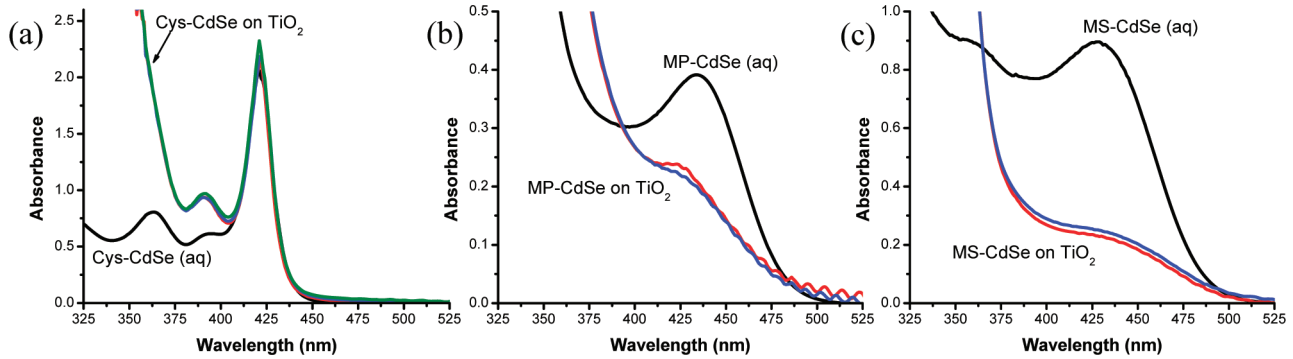

Figure 3. Representative absorption spectra of aqueous reaction mixtures containing (a) Cys-CdS, (b) MP-CdSe, and (c) MS-CdSe (black spectra) and of nanocrystalline TiO_2 films after immersion in the reaction mixtures for 16 h (colored spectra).

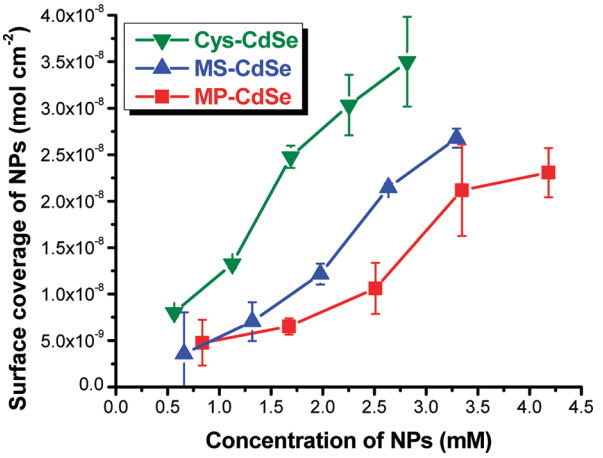

Figure 4. Equilibrium binding data for adsorption of Cys-CdSe, MS-CdSe, and MP-CdSe to nanocrystalline TiO_2 films. Error bars represent the standard deviation of measurements on 4 films.

of Cys to the (110) surface of rutile TiO_2.[101] Cys adsorbed to TiO_2 primarily by coordination of the carboxylate to surface Ti^{4+} sites; a secondary interaction involved the thiolate. The amine did not coordinate to the surface but became protonated at high surface coverages. We assume that thiolates of Cys were coordinated to surface Cd^{2+} sites of CdSe, precluding their interaction with TiO_2. Guijarro et al. suggested that free amine groups of CdSe-adsorbed Cys may coordinate to TiO_2, thereby decreasing the CdSe-TiO_2 distance.[49] However, our IR, absorption, and emission data indicate that amines of some or all Cys ligands were coordinated to the CdSe surface. Thus, amines may or may not have been available to bind to TiO_2. Variations of the particle size, monodispersity, and dispersibility of NPs with different capping groups; the fractional surface coverage of capping groups on NPs; and the surface-binding reactivity of free capping groups, which could competitively adsorb to TiO_2, may have contributed to apparent differences in the affinities of Cys-CdSe, MS-CdSe, and MP-CdSe for TiO_2. Such factors complicate the interpretation of trends in equilibrium binding data as a function of the structure of linkers.

Persistence and Degradation of TiO_2-Adsorbed Cys-CdSe in Various Solvents. Immersion of Cys-CdSe-functionalized TiO_2 films in diH_2O caused the diminution, broadening, and red-shift of the first excitonic absorption band (see the Supporting Information, Figure S4a). Under ambient conditions, the absorbance decreased by approximately 20% within 30 min of immersion (see the Supporting Information, Figure S4b). We reported similar spectral changes for dispersed Cys-CdSe NPs upon removal from the synthetic reaction mixture and dilution into basic aqueous solutions.[58] The mechanism involved dissolution of CdSe and formation of solvated cadmium(II)-cysteinato complexes, as well as some particle growth leading to red-shifted absorption. Dispersed Cys-CdSe persisted on long time scales only in the presence of $[Cd(Cys)_3]^{4-}$. Similarly, when Cys-CdSe-functionalized TiO_2 films were immersed in pH 12.5 solutions in which $[Cd(Cys)_3]^{4-}$ was the predominant cadmium(II)-cysteinato complex, the absorption spectrum persisted and the absorbance at λ_{max} did not decrease (see the Supporting Information, Figure S4b). Thus, we assume that, in the absence of $[Cd(Cys)_3]^{4-}$, the spectral changes of TiO_2-adsorbed Cys-CdSe involved dissolution of the NPs through the previously reported mechanism. The absorbance decreased more slowly in Ar-saturated diH_2O than in air-equilibrated diH_2O (Figure S4b), suggesting that oxidation of Cys and/or Se^{2-} accelerated the spectral changes. Desorption of Cys-CdSe may also have contributed to the decreased absorbance in the presence or absence of O_2.

The first excitonic absorption maximum (λ_{max}) of Cys-CdSe-functionalized TiO_2 films varied with the solvent in which films were immersed (see the Supporting Information, Figure S5). The absorption band was furthest red-shifted (λ_{max} of 425−429 nm) for dry films and films immersed in noncoordinating solvents, such as heptane or dichloromethane. The band was furthest blue-shifted (λ_{max} of 422−423 nm) for films in coordinating solvents, such as dimethylsulfoxide and triethylamine. We speculate that the Lewis-basic solvents may have displaced Cys or coordinated to vacant Cd^{2+} sites, shifting Cd^{2+}-centered conduction-band states to higher energies and blue-shifting the excitonic absorption.

Photoelectrochemistry of QDSSCs. Short-circuit photocurrent action spectra (IPCE vs wavelength) were acquired for TiO_2 films coated with Cys-CdSe, MP-CdSe, or MS-CdSe (Figure 5). For all three sensitizers, photocurrent onsets were red-shifted significantly relative to the absorption onset of TiO_2. Photocurrent action spectra coincided closely with absorptance spectra (Figure 5). (Absorptance equals the fraction of photons absorbed, or one minus transmittance.) Thus, excitation of TiO_2-adsorbed Cys-CdSe, MP-CdSe, and MS-CdSe gave rise to sensitized photocurrents. The IPCE at λ_{max} of Cys-CdSe (422 nm) was 0.32 ± 0.05. The absorptance and photocurrent action spectra of TiO_2-adsorbed MP-CdSe and MS-CdSe did not exhibit well-resolved maxima. IPCE values within the first excitonic bands of MP-CdSe and MS-CdSe were 0.14 ± 0.03 (at

422 nm) and 0.10 ± 0.04 (at 428 nm), respectively. Our DSSCs with the N3 dye yielded IPCE values of 0.82 ± 0.07 at the metal-to-ligand charge-transfer absorption maximum (537 nm) (see the Supporting Information, Figure S6), consistent with literature values.[55,102] Reported IPCE values at λ_{max} for QDSSCs prepared by linker-assisted assembly typically range from 0.1 to 0.4, in line with our values.[19,22,41,42,49,103]

The 2−3-fold greater IPCE of Cys-CdSe relative to MP-CdSe and MS-CdSe, under monochromatic illumination at low intensity, arose primarily from increased harvesting of light due to the greater extinction coefficient (Table 1) and higher surface coverage (Figure 4) of Cys-CdSe. Values of absorbed photon-to-current efficiency (APCE), or IPCE divided by absorptance, within the first excitonic absorption band were similar for Cys-CdSe, MP-CdSe, and MS-CdSe (see the Supporting Information, Figure S7). However, rigorous analysis of the relative APCE values was precluded by changes of the absorption spectrum of Cys-CdSe during the measurement of short-circuit photocurrents. The first excitonic absorption band of TiO_2-adsorbed Cys-CdSe decreased, red-shifted, and broadened within 5 min of soaking in the polysulfide electrolyte during the acquisition of data (see the Supporting Information, Figure S8a). (Absorption spectra of TiO_2 films functionalized with MP-CdSe and MS-CdSe changed only minimally (see the Supporting Information, Figure S8b,c).) Thus, the apparent increase of APCE for Cys-CdSe from 440 to 470 nm (see the Supporting Information, Figure S7a) is probably artifactual, arising from decreased and red-shifted absorption rather than from a real increase of APCE in the low-energy tail of the first excitonic absorption band. We speculate that the rapid decrease of excitonic absorbance in the polysulfide electrolyte at short-circuit, which was faster than the decrease of absorbance in basic water (see the Supporting Information, Figure S4), arose from the dissolution of oxidized CdSe. Either an increase of the particle size of CdSe via ripening[58] or the formation of CdS or $CdSe_{1-x}S_x$ via interaction of Cys-CdSe with the polysulfide electrolyte[104] may also have contributed to degradation, as evidenced by the red-shifted absorption band. The observed spectral change complicates the comparison of APCE values as a function of linker functionality from short-circuit photocurrent action spectra acquired at low light intensity. An ongoing challenge is to stabilize Cys-CdSe in the presence of the aqueous polysulfide electrolyte.

Photocurrent-photovoltage ($I-V$) data were acquired under white-light illumination at 56 mW cm^{-2}. DSSCs with N3 were characterized as a reference (see the Supporting Information, Figure S6b). Our measured global energy-conversion efficiency (η) for N3-sensitized TiO_2 was (4.0 ± 0.2)%, approximately 40% of reported η values for N3 DSSCs under simulated AM1.5 solar illumination.[55] Representative data for QDSSCs are shown in Figure 6, and parameters are summarized in Table 2. Under our experimental conditions, η of QDSSCs with Cys-CdSe-functionalized TiO_2 electrodes ((0.45 ± 0.11)%) was approximately 1.2-fold and 6-fold greater than those of QDSSCs with MP-CdSe and MS-CdSe, respectively. The values of η and open-circuit voltage (V_{oc}) for Cys-CdSe are similar to reported values for QDSSCs prepared by linker-assisted assembly,[19,41,42,49,103,105] despite the narrow and blue-shifted excitonic absorption band of Cys-CdSe, which limits light-harvesting. Our η value for MS-CdSe is lower than many reported values for CdSe-based QDSSCs prepared by linker-assisted assembly.[19,41,49,103] The increased η for Cys-CdSe relative to MP-CdSe arose from a 1.3-fold increase of short-circuit photocurrent density (J_{sc}). Both J_{sc} and V_{oc} were significantly greater for Cys-CdSe and MP-CdSe than for MS-CdSe.

Absorbed photon-to-current efficiencies under white-light illumination at short-circuit ($APCE_{WL}$) were estimated from measured J_{sc} values, absorptance spectra, and the measured irradiance spectrum of our white-light source. The calculations are described in Appendix S2 of the Supporting Information; values of $APCE_{WL}$ are presented in Table 2. The average integrated absorbed photon flux of Cys-CdSe-functionalized TiO_2 films was approximately 10% greater than those of TiO_2 films functionalized with MP-CdSe and MS-CdSe (see Appendix

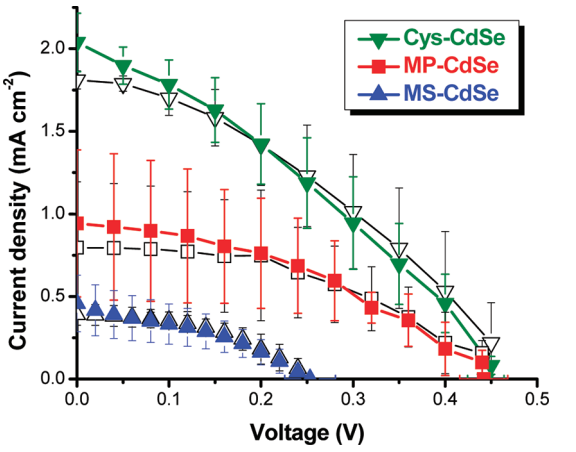

Figure 6. $I-V$ data for QDSSCs with Cys-CdSe, MP-CdSe, and MS-CdSe. Colored data (filled symbols) were acquired in scans from J_{sc} to V_{oc}; black data (open symbols) are from reverse scans. Error bars represent the standard deviation of 6, 4, and 10 measurements for Cys-CdSe, MP-CdSe, and MS-CdSe, respectively.

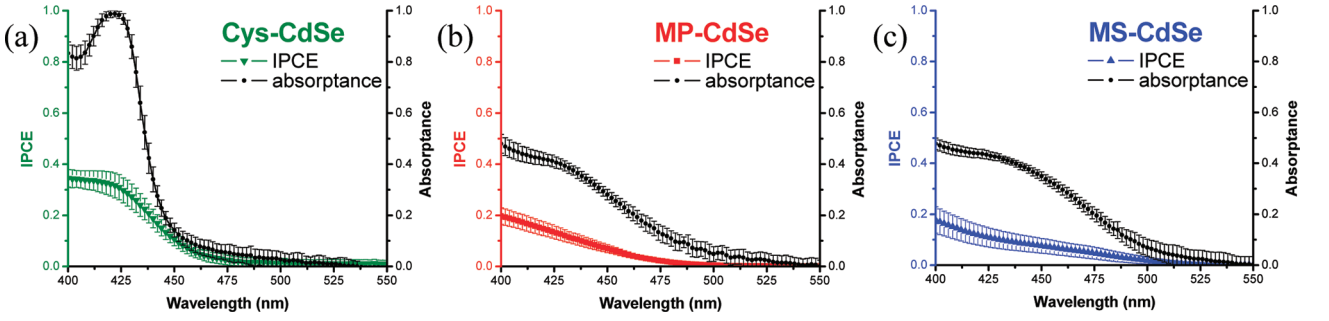

Figure 5. Short-circuit photocurrent action spectra (colored) and absorptance spectra (black) for QDSSCs with (a) Cys-CdSe, (b) MP-CdSe, and (c) MS-CdSe. Error bars represent the standard deviation of 4−5 measurements on 2−3 working electrodes for each sensitizer.

Table 2. Summary of Photocurrent-Photovoltage Data

sensitizer	J_{sc} (mA cm^{-2}) [a,b]	V_{oc} (V) [a,b]	ff [a,c]	η (%) [a,b]	APCE$_{WL}$ [b]
Cys-CdSe	1.6 ± 0.4	0.44 ± 0.02	0.35 ± 0.07	0.45 ± 0.11	0.395 ± 0.067
MP-CdSe	1.2 ± 0.4	0.44 ± 0.03	0.41 ± 0.06	0.38 ± 0.15	0.31 ± 0.13
MS-CdSe	0.45 ± 0.09	0.25 ± 0.03	0.42 ± 0.07	0.08 ± 0.01	0.120 ± 0.035
N3	5.6 ± 1.1	0.81 ± 0.02	0.52 ± 0.09	4.0 ± 0.2	

[a] Standard deviations relative to average of 10−30 measurements (one scan in each direction for 5−15 working electrodes). [b] Abbreviation defined in text. [c] ff = fill factor.

S2). Despite this minimal increase of light-harvesting efficiency, the value of APCE$_{WL}$ for QDSSCs with Cys-CdSe (0.395 ± 0.067) was greater than the values for QDSSCs with MP-CdSe (0.31 ± 0.13) or MS-CdSe (0.120 ± 0.035). APCE equals the product of the electron-injection yield (ϕ_{inj}) and charge-collection efficiency (η_{el}).[106] Therefore, under white-light illumination at 56 mW cm^{-2}, ϕ_{inj} and/or η_{el} for QDSSCs with Cys-CdSe was greater than for QDSSCs with MP-CdSe or MS-CdSe. In contrast, monochromatic APCE values within the first excitonic absorption band, which were measured at lower irradiances, were similar for Cys-CdSe, MP-CdSe, and MS-CdSe (Figure 5 and Figure S7 in the Supporting Information). At higher irradiance, excited-state annihilation processes may have competed with injection of electrons, limiting ϕ_{inj} of MP-CdSe and MS-CdSe. Alternatively, as the amount of injected electrons increased with irradiance, recombination of injected electrons with CdSe-localized holes may have competed more efficiently with charge collection, limiting η_{el}. Durrant and co-workers have shown that, for N3-sensitized nanocrystalline TiO_2 films, the charge-recombination rate increases by several orders of magnitude with increasing occupation of conduction-band or electron-trap states in TiO_2.[107] Regardless of the mechanism, our I−V measurements clearly indicate that, at irradiances approaching that of the solar spectrum, ϕ_{inj} and/or η_{el} were greater for TiO_2 films sensitized with Cys-CdSe compared to MP-CdSe and MS-CdSe. The effect probably arose from differences in the electronic properties of Cys-CdSe MSCs relative to MP-CdSe and MS-CdSe QDs or from differences in the electronic properties of the linkers.

Transient Absorption Spectroscopy. To investigate further the differences in electron-transfer reactivity, we acquired transient absorbance (TA) data for Cys-CdSe in Ar-saturated aqueous dispersions and for Cys-CdSe and MS-CdSe adsorbed to nanocrystalline TiO_2 and ZrO_2 films immersed in Ar-saturated ethylene glycol. TA data were acquired after pulsed excitation at 415 nm. At delay times of several hundred nanoseconds and longer, the TA spectrum of Cys-CdSe in pH-12.5 aqueous dispersions consisted of an intense bleach centered at ~430 nm and a broad and weak absorption beyond 450 nm (see the Supporting Information, Figure S9). (The TA spectrum may have contained a weak absorption at wavelengths shorter than 400 nm; however, standard deviations of $\Delta A/A$ were large because of the low transmittance of the sample at short wavelengths.) We attribute the bleach to population of the lowest-energy excitonic state (1S(e)−1S(h)).[108] Higher-energy excitonic states of CdS and CdSe QDs typically relax to the first excitonic state within 1×10^{-13} to 1×10^{-11} s, giving rise to a narrow bleach within the low-energy region of the ground-state absorption spectrum, similar to our observed bleach for Cys-CdSe.[109−113] Broad and long-lived transient absorptions in the red and near-IR for cadmium chalcogenide QDs in aqueous dispersions have been attributed to trapped electrons, trapped holes, and hydrated electrons.[114−118] Our long-wavelength transient absorption for Cys-CdSe probably arose from a combination of such signals.

ZrO_2 is an inert substrate for molecular dyes and QDs due to its highly negative conduction band-edge potential (E_c),[119,120] which renders electron injection thermodynamically unfavorable.[28,121−124] UV/vis absorption spectra of ZrO_2 films functionalized with Cys-CdSe and MS-CdSe were similar to the spectra of corresponding CdSe-modified TiO_2 films (see the Supporting Information, Figure S10). The value of λ_{max} for Cys-CdSe on ZrO_2 was unshifted relative to TiO_2. (ZrO_2 and TiO_2 films functionalized with MS-CdSe did not exhibit excitonic maxima.) Surface coverages of Cys-CdSe and MS-CdSe were slightly lower on ZrO_2 than on TiO_2; average absorbances at 415 nm, the excitation wavelength in transient absorption experiments, were 17 and 30% lower for Cys-CdSe and MS-CdSe, respectively, on ZrO_2 relative to TiO_2. Measured TA differences were normalized to ground-state absorbances at 415 nm to minimize artifactual effects arising from substrate-dependent differences in ground-state spectra of adsorbed CdSe NPs.

The TA spectrum of Cys-CdSe adsorbed to ZrO_2, acquired 500 ns after excitation into the first excitonic transition of CdSe, consisted of a broad and featureless absorption extending from 460 nm into the near-IR (Figure 7a). The absorption decayed only minimally within ten microseconds (Figure 8). A bleach was measurable at probe wavelengths within the first excitonic transition; however, signal-to-noise was poor because of the low transmittance of samples. Therefore, we focus on the long-wavelength region of the TA spectrum. The lack of significant changes of the TA spectrum of Cys-CdSe upon attachment to ZrO_2 indicates that ZrO_2 was an inert substrate and that photophysics of Cys-CdSe were minimally perturbed at high local concentrations on surfaces. The E_c of bulk ZrO_2 is −1.25 V vs SCE,[119,120] approximately 850 mV negative of E_c of bulk CdSe and 950 mV negative of E_c of bulk TiO_2.[125,126] Calculating the relative driving forces for electron injection into ZrO_2 and TiO_2 is complicated by the effects of quantum confinement, solvation, and the existence of distributions of trap states, which affect the energy and density of potential donor and acceptor states. At a minimum, the driving force for electron injection into ZrO_2 was nearly 1 V less than for injection into TiO_2. Our data suggest that electron injection into ZrO_2 was negligible.

The long-wavelength transient absorption for Cys-CdSe on TiO_2 was significantly more intense than that of Cys-CdSe on ZrO_2 (Figure 7a). Electrons in conduction-band or electron-trap states of TiO_2 exhibit a broad absorption from the visible into the near-IR, which arises from an interband transition.[127−129] Such transient absorptions following excitation of TiO_2-adsorbed dyes have been correlated with electron injection.[122,130] Therefore, we

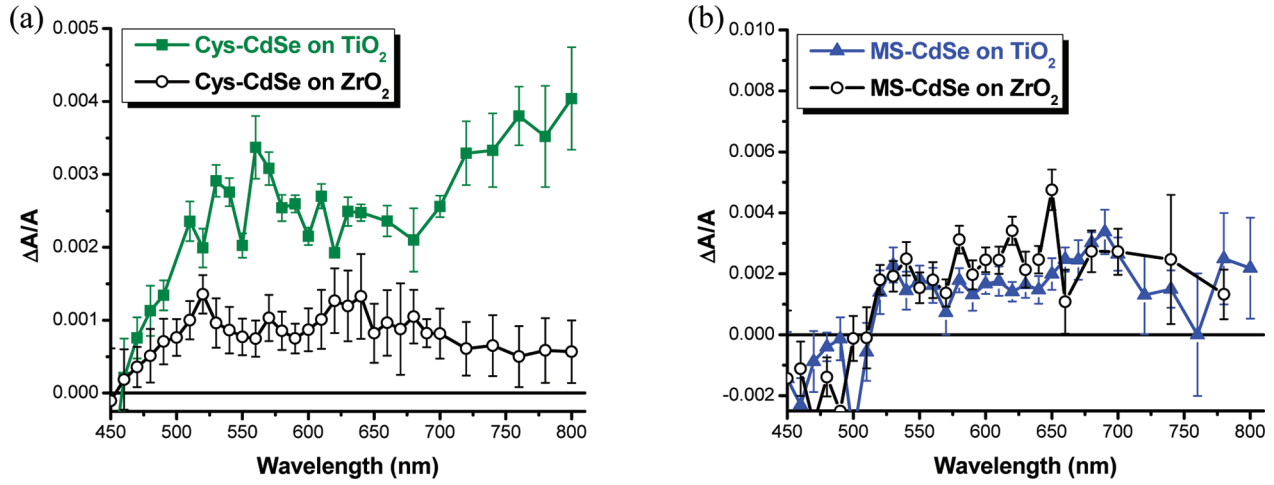

Figure 7. TA spectra fo (a)r Cys-CdSe and (b) MS-CdSe on TiO_2 and ZrO_2 films immersed in Ar-saturated ethylene glycol. Data were acquired 500 ns after pulsed excitation at 415 nm. Error bars correspond to the propagation of the standard deviations of 100 measured values of $\Delta A/A$ within ±50 ns of the 500 ns delay times from single-wavelength decay traces from 3 to 5 films.

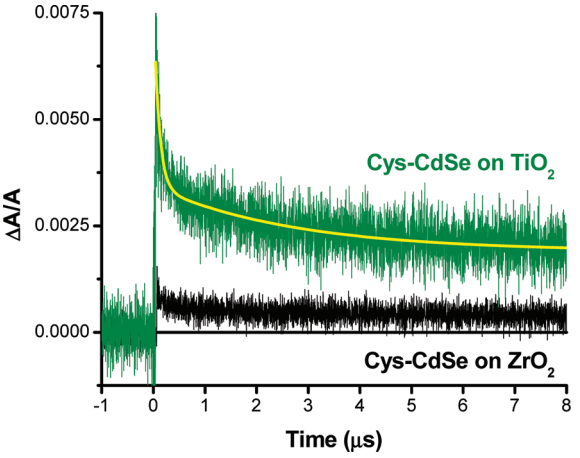

Figure 8. TA decay traces at 760 nm for Cys-CdSe on TiO_2 and ZrO_2 films immersed in Ar-saturated ethylene glycol after pulsed excitation at 415 nm. The yellow line on the data for Cys-CdSe on TiO_2 is a biexponential fit (eq 1).

attribute the significantly increased TA beyond 460 nm for Cys-CdSe on TiO_2, relative to ZrO_2, to the interband transition of injected electrons. TA decay traces (Figure 8) were modeled by the biexponential function

$$\Delta A/A = C_1\exp(-t/\tau_1) + C_2\exp(-t/\tau_2) + (\Delta A/A)_0 \quad (1)$$

where $\Delta A/A$ is the normalized absorbance difference, C_1 and C_2 are preexponential weighting factors, t is time, τ_1 and τ_2 are the lifetimes, and $(\Delta A/A)_0$ is the normalized absorbance difference to which data decayed on long time scales. Average lifetimes were calculated as

$$\langle\tau\rangle = \frac{\sum_n (C_n\tau_n^2)}{\sum_n (C_n\tau_n)} \quad (2)$$

where n corresponds to the nth component of a given multiexponential decay process.[131−135] A fit is overlaid on the data for Cys-CdSe on TiO_2 in Figure 8. The average lifetime $((2.5 \pm 0.2) \times 10^{-6}$ s) is an approximate indication of the time scale of charge recombination following electron injection, which is similar to recombination time scales for molecularly linked CdS-TiO_2 assemblies.[28,29] However, in our data for Cys-CdSe on TiO_2, the decay of the underlying absorption from trapped or solvated charges may also have influenced the measured kinetics.

TA spectra were acquired for MS-CdSe adsorbed to TiO_2 and ZrO_2 films following pulsed excitation at 415 nm, within the first excitonic transition of MS-CdSe (Figure 7b). Remarkably, spectra for MS-CdSe on the two substrates were nearly superimposable on time scales from 500 ns to 10 μs. Therefore, on these time scales, TA data provide no evidence for electrons in TiO_2 following pulsed excitation of MS-CdSe.

The significant differences in TA data for MS-CdSe and Cys-CdSe could, in principle, be attributed to differences in ϕ_{inj} and/or charge-recombination kinetics. That is, the lack of electrons in TiO_2 within 500 ns after excitation of MS-CdSe could have arisen from inefficient injection, rapid recombination, or both. Mora-Seró et al. reported faster electron injection at CdSe-TiO_2 interfaces with cysteine as linker relative to 4-mercaptobenzoic acid or 3-mercaptopropionic acid.[49] They attributed the result to decreased interparticle distance and improved electronic coupling relative to nonaminated linkers. A similar effect may have increased ϕ_{inj} of Cys-CdSe relative to MS-CdSe in our samples. Alternatively, the excitonic states and electron-trap states of Cys-CdSe MSCs were at more negative potentials than those of MS-CdSe QDs, as evidenced by the blue-shifted absorption, band-edge emission, and trap-state emission of Cys-CdSe (Figure 1). Thus, the increased driving force for electron injection may have contributed to increased ϕ_{inj}.

Notably, our photoelectrochemical data (Figure 5c) provide clear evidence for MS-CdSe-sensitized photocurrent; therefore, ϕ_{inj} for MS-CdSe was nonzero, and the measured differences in TA data must also have arisen from differences in charge-recombination kinetics. It follows that charge recombination at the MS-CdSe/TiO_2 interface was rapid and complete within 500 ns in the absence of the polysulfide electrolyte and an external circuit. We speculate that the electronic properties of the linkers influenced the stability of the charge-separated states and,

therefore, the charge-recombination kinetics. The amine group of Cys, which was coordinated to Cd^{2+} sites of CdSe, may have stabilized the hole on CdSe following electron injection. MS lacks the amine group. Moreover, if both carboxylates of MS were coordinated to TiO_2, the additional negative charge at the TiO_2 surface may have further destabilized the charge-separated state, in which electrons are localized in TiO_2 following injection. Finally, the significant differences in the energies and densities of trap states of Cys-CdSe and MS-CdSe, as evidenced by differences in emission spectra (Figure 1), may have affected the mechanism and kinetics of charge recombination.

CONCLUSIONS

The structure and functionality of native capping groups of water-dispersible CdSe NPs influenced their electronic properties, their affinity for TiO_2, and the electron-transfer reactivity of CdSe-TiO_2 interfaces. Cys promoted the formation of MSCs with narrow and intense first excitonic absorption bands, whereas MP and MS promoted the formation of regular QDs with broader and red-shifted absorption. Our FTIR data and pH-dependent electronic spectra indicate that the amine of Cys coordinated to Cd^{2+} surface sites of Cys-CdSe, leading to narrow excitonic absorption, enhanced band-edge emission, and blue-shifted trap-state emission relative to MP-CdSe and MS-CdSe.

Our all-aqueous chemistry provides a simple and "green" method for tethering NPs to surfaces. "Method 2" assembly, in which native capping groups serve as molecular linkers, involves just one surface-functionalization step, thereby streamlining linker-assisted materials assembly and potentially improving reproducibility. We found that Cys-CdSe and MS-CdSe exhibited higher surface coverages than MP-CdSe on TiO_2. The additional Lewis-basic functional groups of Cys and MS may have increased their affinities for TiO_2.

QDSSCs with Cys-CdSe were more efficient than those with MP-CdSe or MS-CdSe. Our TA data indicate that charge recombination was vastly slower, and that electron injection was probably more efficient, at Cys-CdSe/TiO_2 interfaces than at MS-CdSe/TiO_2 interfaces. The combined effects of slower recombination, which translates to improved charge collection in QDSSCs, and more efficient electron injection gave rise to the measured 1.3−3.3-fold increase of $APCE_{WL}$ and 1.2-to-6-fold increase of η for Cys-CdSe relative to MP-CdSe and MS-CdSe.

In summary, Cys is an intriguing linker, and aqueous method-2 assembly is promising. However, an ongoing challenge is to stabilize Cys-capped CdSe NPs on surfaces, such that they resist degradation in water and aqueous electrolytes. In addition, while the electron-transfer reactivity of CdSe MSCs is of fundamental interest in light of their unique electronic properties, their high-energy excitonic transitions are not practical for real-world light-harvesting applications. Thus, the materials-assembly chemistry and electron-transfer reactivity of Cys-capped NPs with improved light-harvesting properties warrant further investigation.

ASSOCIATED CONTENT

Supporting Information. Additional experimental methods, XRD data, FTIR data, electronic spectra of dispersed and TiO_2-adsorbed CdSe NPs under various conditions, photoelectrochemical data for N3-sensitized TiO_2, APCE data for CdSe-functionalized TiO_2, TA data for dispersed Cys-CdSe, and description of calculations of $APCE_{WL}$. This material is available free of charge via the Internet at http://pubs.acs.org.

AUTHOR INFORMATION

Corresponding Author
*E-mail: dwatson3@buffalo.edu.

ACKNOWLEDGMENT

This work was supported by the National Science Foundation (CHE-0645678).

REFERENCES

(1) Brus, L. E. *J. Chem. Phys.* **1984**, *80*, 4403–4409.
(2) Larson, D. R.; Zipfel, W. R.; Williams, R. M.; Clark, S. W.; Bruchez, M. P.; Wise, F. W.; Webb, W. W. *Science* **2003**, *300*, 1434–1436.
(3) Sambur, J. B.; Riha, S. C.; Choi, D.; Parkinson, B. A. *Langmuir* **2010**, *26*, 4839–4847.
(4) Nozik, A. J. *Physica E* **2002**, *14*, 115–120.
(5) Schaller, R. D.; Klimov, V. I. *Phys. Rev. Lett.* **2004**, *92*, 186601.
(6) Ellingson, R. J.; Beard, M. C.; Johnson, J. C.; Yu, P.; Micic, O. I.; Nozik, A. J.; Shabaev, A.; Efros, A. L. *Nano Lett.* **2005**, *5*, 865–871.
(7) Nozik, A. J. *Chem. Phys. Lett.* **2008**, *457*, 3–11.
(8) McGuire, J. A.; Joo, J.; Pietryga, J. M.; Schaller, R. D.; Klimov, V. I. *Acc. Chem. Res.* **2008**, *41*, 1810–1819.
(9) Midgett, A. G.; Hillhouse, H. W.; Hughes, B. K.; Nozik, A. J.; Beard, M. C. *J. Phys. Chem. C* **2010**, *114*, 17486–17500.
(10) Beard, M. C. *J. Phys. Chem. Lett.* **2011**, *2*, 1282–1288.
(11) Kamat, P. V. *J. Phys. Chem. C* **2008**, *112*, 18737–18753.
(12) Shockley, W.; Queisser, H. J. *J. Appl. Phys.* **1961**, *32*, 510–519.
(13) Sambur, J. B.; Novet, T.; Parkinson, B. A. *Science* **2010**, *330*, 63–66.
(14) Hodes, G. *J. Phys. Chem. C* **2008**, *112*, 17778–17787.
(15) Niitsoo, O.; Sarkar, S. K.; Pejoux, C.; Rühle, S.; Cahen, D.; Hodes, G. *J. Photochem. Photobiol., A* **2006**, *181*, 306–313.
(16) Vogel, R.; Hoyer, P.; Weller, H. *J. Phys. Chem.* **1994**, *98*, 3183–3188.
(17) Lee, H. J.; Chen, P.; Moon, S.-J.; Sauvage, F.; Sivula, K.; Bessho, T.; Gamelin, D. R.; Comte, P.; Zakeeruddin, S. M.; Seaok, S. I.; Grätzel, M.; Nazeeruddin, M. K. *Langmuir* **2009**, *25*, 7602–7608.
(18) Yu, P.; Zhu, K.; Norman, A. G.; Ferrere, S.; Frank, A. J.; Nozik, A. J. *J. Phys. Chem. B* **2006**, *110*, 25451–25454.
(19) Giménez, S.; Mora-Seró, I.; Macor, L.; Guijarro, N.; Lana-Villarreal, T.; Gómez, R.; Diguna, L. J.; Shen, Q.; Toyoda, T.; Bisquert, J. *Nanotechnology* **2009**, *20*, 295204.
(20) Guijarro, N.; Lana-Villarreal, T.; Mora-Seró, I.; Gómez, R. *J. Phys. Chem. C* **2009**, *113*, 4208–4214.
(21) Watson, D. F. *J. Phys. Chem. Lett.* **2010**, *1*, 2299–2309.
(22) Robel, I.; Subramanian, V.; Kuno, M.; Kamat, P. V. *J. Am. Chem. Soc.* **2006**, *128*, 2385–2393.
(23) Dibbell, R. S.; Soja, G. R.; Hoth, R. M.; Watson, D. F. *Langmuir* **2007**, *23*, 3432–3439.
(24) Mann, J. R.; Watson, D. F. *Langmuir* **2007**, *23*, 10924–10928.
(25) Chang, C.-H.; Lee, Y.-L. *Appl. Phys. Lett.* **2007**, *91*, 053503.
(26) Lee, Y.-L.; Lo, Y.-S. *Adv. Funct. Mater.* **2009**, *19*, 604–609.
(27) Hyun, B.-R.; Zhong, Y.-W.; Bartnik, A. C.; Sun, L.; Abruña, H. D.; Wise, F. W.; Goodreau, J. D.; Matthews, J. R.; Leslie, T. M.; Borrelli, N. F. *ACS Nano* **2008**, *2*, 2206–2212.
(28) Dibbell, R. S.; Watson, D. F. *J. Phys. Chem. C* **2009**, *113*, 3139–3149.
(29) Dibbell, R. S.; Youker, D. G.; Watson, D. F. *J. Phys. Chem. C* **2009**, *25*, 18643–18651.
(30) Lawless, D.; Kapoor, S.; Meisel, D. *J. Phys. Chem.* **1995**, *99*, 10329–10335.
(31) Bakkers, E. P. A. M.; Marsman, A. W.; Jenneskens, L. W.; Vanmaekelbergh, D. *Angew. Chem., Int. Ed.* **2000**, *39*, 2297–2299.

(32) Bakkers, E. P. A. M.; Roest, A. L.; Marsman, A. W.; Jenneskens, L. W.; de Jong-van Steensel, L. I.; Kelly, J. J.; Vanmaekelbergh, D. *J. Phys. Chem. B* **2000**, *104*, 7266–7272.
(33) Robel, I.; Kuno, M.; Kamat, P. *J. Am. Chem. Soc.* **2007**, *129*, 4136–4137.
(34) Bang, J. H.; Kamat, P. V. *ACS Nano* **2009**, *3*, 1467–1476.
(35) Chakrapani, V.; Tvrdy, K.; Kamat, P. V. *J. Am. Chem. Soc.* **2010**, *132*, 1228–1229.
(36) Jin, S.; Lian, T. *Nano Lett.* **2009**, *9*, 2448–2454.
(37) Leventis, H. C.; O'Mahony, F.; Akhtar, J.; Afzaal, M.; O'Brien, P.; Haque, S. A. *J. Am. Chem. Soc.* **2010**, *132*, 2743–2750.
(38) Hyun, B.-R.; Bartnik, A. C.; Sun, L.; Hanrath, T.; Wise, F. W. *Nano Lett.* **2011**, *11*, 2126–2132.
(39) Zaban, A.; Mićić, O. I.; Gregg, B. A.; Nozik, A. J. *Langmuir* **1998**, *14*, 3153–3156.
(40) Kongkanand, A.; Tvrdy, K.; Takechi, K.; Kuno, M.; Kamat, P. V. *J. Am. Chem. Soc.* **2008**, *130*, 4007–4015.
(41) Lee, J. H.; Yum, J.-H.; Leventis, H. C.; Zakeeruddin, S. M.; Haque, S. A.; Chen, P.; Seok, S. I.; Grätzel, M.; Nazeeruddin, M. K. *J. Phys. Chem. C* **2008**, *112*, 11600–11608.
(42) Mora-Seró, I.; Giménez, S.; Moehl, T.; Fabregat-Santiago, F.; Lana-Villarreal, T.; Gómez, R.; Bisquert, J. *Nanotechnology* **2008**, *19*, 424007.
(43) Leschkies, K. S.; Divakar, R.; Basu, J.; Enache-Pommer, E.; Boercker, J. E.; Carter, C. B.; Kortshagen, U. R.; Norris, D. J.; Aydil, E. S. *Nano Lett.* **2007**, *7*, 1793–1798.
(44) Mora-Seró, I.; Bisquert, J.; Dittrich, T.; Belaidi, A.; Susha, A. S.; Rogach, A. L. *J. Phys. Chem. C* **2007**, *111*, 14889–14892.
(45) Sambur, J. B.; Parkinson, B. A. *J. Am. Chem. Soc.* **2010**, *132*, 2130–2131.
(46) Cao, X.; Chen, P.; Guo, Y. *J. Phys. Chem. C* **2008**, *112*, 20560–20566.
(47) Kuo, K.-T.; Liu, D.-M.; Chen, S.-Y.; Lin, C.-C. *J. Mater. Chem.* **2009**, *19*, 6780–6788.
(48) Gao, X.-F.; Li, H.-B.; Sun, W.-T.; Chen, Q.; Tang, F.-Q.; Peng, L.-M. *J. Phys. Chem. C* **2009**, *113*, 7531–7535.
(49) Guijarro, N.; Shen, Q.; Giménez, S.; Mora-Seró, I.; Bisquert, J.; Lana-Villarreal, T.; Toyoda, T.; Gómez, R. *J. Phys. Chem. C* **2010**, *114*, 22352–22360.
(50) Park, Y.-S.; Dmytruk, A.; Dmitruk, I.; Yasuto, N.; Kasuya, A.; Takeda, M.; Ohuchi, N. *J. Nanosci. Nanotech* **2007**, *7*, 3750–3753.
(51) Park, Y.-S.; Dmytruk, A.; Dmitruk, I.; Kasuya, A.; Takeda, M.; Ohuchi, N.; Okamoto, Y.; Kaji, N.; Tokeshi, M.; Baba, Y. *ACS Nano* **2010**, *4*, 121–128.
(52) Heimer, T. A.; D'Arcangelis, S. T.; Farzad, F.; Stipkala, J. M.; Meyer, G. J. *Inorg. Chem.* **1996**, *35*, 5319–5324.
(53) Smith, A. R.; Watson, D. F. *Chem. Mater.* **2010**, *22*, 294–304.
(54) Tachibana, Y.; Umekita, K.; Otsuka, Y.; Kuwabata, S. *J. Phys. D: Appl. Phys.* **2008**, *41*, 102002.
(55) Nazeeruddin, M. K.; Kay, A.; Rodicio, I.; Humphry-Baker, R.; Müller, E.; Liska, P.; Vlachopoulos, N.; Grätzel, M. *J. Am. Chem. Soc.* **1993**, *115*, 6382–6390.
(56) Mann, J. R.; Gannon, M. K.; Fitzgibbons, T. C.; Detty, M. R.; Watson, D. F. *J. Phys. Chem. C* **2008**, *112*, 13057–13061.
(57) Tachan, Z.; Shalom, M.; Hod, I.; Rühle, S.; Tirosh, S.; Zaban, A. *J. Phys. Chem. C* **2011**, *115*, 6162–6166.
(58) Baker, J. S.; Nevins, J. S.; Coughlin, K. M.; Colón, L. A.; Watson, D. F. *Chem. Mater.* **2011**, *23*, 3546–3555.
(59) Murray, C. B.; Norris, D. J.; Bawendi, M. G. *J. Am. Chem. Soc.* **1993**, *115*, 8706–8715.
(60) Yu, W. W.; Qu, L.; Guo, W.; Peng, X. *Chem. Mater.* **2003**, *15*, 2854–2860.
(61) Ptatschek, V.; Schmidt, T.; Lerch, M.; Müller, G.; Spanhel, L. *Ber. Bunsenges. Phys. Chem.* **1998**, *102*, 85–95.
(62) Soloviev, V. N.; Eichhöfer, A.; Fenske, D.; Banin, U. *J. Am. Chem. Soc.* **2000**, *122*, 2673–2674.
(63) Soloviev, V. N.; Eichhöfer, A.; Fenske, D.; Banin, U. *J. Am. Chem. Soc.* **2001**, *123*, 2354–2364.
(64) Landes, C.; Braun, M.; Burda, C.; El-Sayed, M. A. *Nano Lett.* **2001**, *1*, 667–670.
(65) Kasuya, A.; Sivamohan, R.; Barnakov, Y. A.; Dmitruk, I. M.; Nirasawa, T.; Romanyuk, V. R.; Kumar, V.; Mamykin, S. V.; Tohji, K.; Jeyadevan, B.; Shinoda, K.; Kudo, T.; Terasaki, O.; Liu, Z.; Belosludov, R. V.; Sundararajan, V.; Kawazoe, Y. *Nat. Mater.* **2004**, *3*, 99–102.
(66) Kudera, S.; Zanella, M.; Giannini, C.; Rizzo, A.; Li, Y.; Gigli, G.; Cingolani, R.; Ciccarella, G.; Spahl, W.; Parak, W. J.; Manna, L. *Adv. Mater.* **2007**, *19*, 548–552.
(67) Ouyang, J.; Zaman, M. B.; Yan, F. J.; Johnston, D.; Li, G.; Wu, X.; Leek, D.; Ratcliffe, C. I.; Ripmeester, J. A.; Yu, K. *J. Phys. Chem. C* **2008**, *112*, 13805–13811.
(68) Park, Y.-S.; Dmytruk, A.; Dmitruk, I.; Kasuya, A.; Okamoto, Y.; Kaji, N.; Tokeshi, M.; Baba, Y. *J. Phys. Chem. C* **2010**, *114*, 18834–18840.
(69) Yu, K.; Hu, M. Z.; Wang, R.; Le Piolet, M.; Frotey, M.; Zaman, M. B.; Wu, X.; Leek, D. M.; Tao, Y.; Wilkinson, D.; Li, C. *J. Phys. Chem. C* **2010**, *114*, 3329–3339.
(70) Underwood, D. F.; Kippeny, T.; Rosenthal, S. J. *J. Phys. Chem. B* **2001**, *105*, 436–443.
(71) Ramsden, J. J.; Grätzel, M. *J. Chem. Soc., Faraday Trans.* **1984**, *80*, 919–933.
(72) Hässelbarth, A.; Eychmüller, A.; Weller, H. *Chem. Phys. Lett.* **1993**, *203*, 271–276.
(73) Tata, M.; Banerjee, S.; John, V. T.; Waguespack, Y.; McPherson, G. L. *Colloids Surf., A* **1997**, *127*, 39–46.
(74) Bowen Katari, J. E.; Colvin, V. L.; Alivisatos, A. P. *J. Phys. Chem.* **1994**, *98*, 4109–4117.
(75) Peng, Z. A.; Peng, X. *J. Am. Chem. Soc.* **2001**, *123*, 183–184.
(76) Shindo, H.; Brown, T. L. *J. Am. Chem. Soc.* **1965**, *87*, 1904–1909.
(77) Sze, Y. K.; Davis, A. R.; Neville, G. A. *Inorg. Chem.* **1975**, *14*, 1969–1974.
(78) Jalilehvand, F.; Mah, V.; Leung, B. O.; Mink, J.; Bernard, G. M.; Hajba, L. *Inorg. Chem.* **2009**, *48*, 4219–4230.
(79) Condrate, R. A.; Nakamoto, K. *J. Chem. Phys.* **1965**, *42*, 2590–2598.
(80) Nakamoto, K. *Infrared and Raman Spectra of Inorganic and Coordination Compounds*. 5th ed.; John Wiley and Sons: New York, 1997.
(81) *CRC Handbook of Chemistry and Physics*, 84th ed.; Lide, D. R., Ed.; CRC Press: New York, 2003−2004.
(82) Barrie, P. J.; Gyani, A.; Motevalli, M.; O'Brien, P. *Inorg. Chem.* **1993**, *32*, 3862–3867.
(83) Lee, J. H.; Kim, Y. A.; Kim, K.; Huh, Y. D.; Hyun, J. W.; Kim, H. S.; Noh, S. J.; Hwang, C.-S. *Bull. Korean Chem. Soc.* **2007**, *28*, 1091–1096.
(84) Nakamoto, K.; Morimoto, Y.; Martell, A. E. *J. Am. Chem. Soc.* **1961**, *83*, 4528–4532.
(85) Deacon, G. B.; Phillips, R. J. *Coord. Chem. Rev.* **1980**, *33*, 227–250.
(86) Carty, A. J.; Taylor, N. J. *Inorg. Chem.* **1977**, *16*, 177–181.
(87) Dannhauser, T.; O'Neil, M.; Johansson, K.; Whitten, D.; McLendon, G. *J. Phys. Chem.* **1986**, *90*, 6074–6076.
(88) Cowdery-Corvan, J. R.; Whitten, D. G.; McLendon, G. L. *Chem. Phys.* **1993**, *176*, 377–386.
(89) Talapin, D. V.; Rogach, A. L.; Kornowski, A.; Haase, M.; Weller, H. *Nano Lett.* **2001**, *1*, 207–211.
(90) Bullen, C.; Mulvaney, P. *Langmuir* **2006**, *22*, 3007–3013.
(91) Kim, W.; Lim, S. J.; Jung, S.; Shin, S. K. *J. Phys. Chem. C* **2010**, *114*, 1539–1546.
(92) Jalilehvand, F.; Leung, B. O.; Mah, V. *Inorg. Chem.* **2009**, *48*, 5758–5771.
(93) Finnie, K. S.; Bartlett, J. R.; Woolfrey, J. L. *Langmuir* **1998**, *14*, 2744–2749.
(94) Shklover, V.; Ovchinnkov, Y. E.; Braginsky, L. S.; Zakeeruddin, S. M.; Grätzel, M. *Chem. Mater.* **1998**, *10*, 2533–2541.
(95) Fillinger, A.; Parkinson, B. A. *J. Electrochem. Soc.* **1999**, *146*, 4559–4564.

(96) Nazeeruddin, M. K.; Humphry-Baker, R.; Liska, P.; Grätzel, M. *J. Phys. Chem. B* **2003**, *107*, 8981–8987.
(97) Trammell, S. A.; Meyer, T. J. *J. Phys. Chem. B* **1999**, *103*, 104–107.
(98) Watson, D. F.; Marton, A.; Stux, A. M.; Meyer, G. J. *J. Phys. Chem. B* **2004**, *108*, 11680–11688.
(99) Hoertz, P. G.; Staniszewski, A.; Marton, A.; Higgins, G. T.; Incarvito, C. D.; Rheingold, A. L.; Meyer, G. J. *J. Am. Chem. Soc.* **2006**, *128*, 8234–8245.
(100) Mann, J. R.; Nevins, J. S.; Soja, G. R.; Wells, D. D.; Levy, S. C.; Marsh, D. A.; Watson, D. F. *Langmuir* **2009**, *25*, 12217–12228.
(101) Ataman, E.; Isvoranu, C.; Knudsen, J.; Schulte, K.; Andersen, J. N.; Schnadt, J. *Surf. Sci.* **2011**, *605*, 179–186.
(102) Nazeeruddin, M. K.; Péchy, P.; Renouard, T.; Zakeeruddin, S. M.; Humphry-Baker, R.; Comte, P.; Liska, P.; Cevey, L.; Costa, E.; Shklover, V.; Spiccia, L.; Deacon, G. B.; Bignozzi, C.; Grätzel, M. *J. Am. Chem. Soc.* **2001**, *123*, 1613–1624.
(103) Chen, J.; Song, J. L.; Sun, X. W.; Deng, W. Q.; Jiang, C. Y.; Lei, W.; Huang, J. H.; Liu, R. S. *Appl. Phys. Lett.* **2009**, *94*, 153115.
(104) Chakrapani, V.; Baker, D.; Kamat, P. V. *J. Am. Chem. Soc.* **2011**, *133*, 9607–9615.
(105) Chakrapani, V.; Baker, D.; Kamat, P. V. *J. Am. Chem. Soc.* **2010**, *133*, 9607–9615.
(106) Watson, D. F.; Meyer, G. J. *Annu. Rev. Phys. Chem.* **2005**, *56*, 119–156.
(107) Haque, S. A.; Tachibana, Y.; Willis, R. L.; Moser, J. E.; Grätzel, M.; Klug, D. R.; Durrant, J. R. *J. Phys. Chem. B* **2000**, *104*, 538–547.
(108) Ekimov, A. I.; Hache, F.; Schanne-Klein, M. C.; Ricard, D.; Flytzanis, C.; Kudryavtsev, I. A.; Yazeva, T. V.; Rodina, A. V.; Efros, A. L. *J. Opt. Soc. Am. B: Opt. Phys.* **1993**, *10*, 100–107.
(109) Hilinski, E. F.; Lucas, P. A.; Wang, Y. *J. Chem. Phys.* **1988**, *89*, 3435–3441.
(110) Bawendi, M. G.; Wilson, W. L.; Rothberg, L.; Carroll, P. J.; Jedju, T. M.; Steigerwald, M. L.; Brus, L. E. *Phys. Rev. Lett.* **1990**, *65*, 1623–1626.
(111) Klimov, V. I.; Haring-Bolivar, P.; Kurz, H.; Karavanskii, V. A. *Superlattices Microstruct.* **1996**, *20*, 395–404.
(112) Logunov, S.; Green, T.; Marguet, S.; El-Sayed, M. A. *J. Phys. Chem.* **1998**, *102*, 5652–5658.
(113) Burda, C.; Link, S.; Green, T. C.; El-Sayed, M. A. *J. Phys. Chem. B* **1999**, *103*, 10775–10780.
(114) Zhang, J. Z.; O'Neil, R. H.; Roberti, T. W. *J. Phys. Chem.* **1994**, *98*, 3859–3864.
(115) Roberti, T. W.; Cherepy, N. J.; Zhang, J. Z. *J. Chem. Phys.* **1998**, *108*, 2143–2151.
(116) Zhang, J. Z. *J. Phys. Chem. B* **2000**, *104*, 7239–7253.
(117) Uchihara, T.; Urasaki, T.; Kamiya, T.; Tamaki, Y.; Ganeko, M.; Kinjo, S.; Oshiro, H.; Kinjo, A. *J. Photochem. Photobiol., A* **1998**, *118*, 131–136.
(118) Uchihara, T.; Kamiya, T.; Maedomari, S.; Maehira, S.; Kinjo, A. *J. Photochem. Photobiol., A* **2001**, *141*, 193–199.
(119) Sayama, K.; Arakawa, H. *J. Phys. Chem.* **1993**, *97*, 531–533.
(120) Sayama, K.; Arakawa, H. *J. Photochem. Photobiol., A* **1996**, *94*, 67–76.
(121) Kay, A.; Humphry-Baker, R.; Grätzel, M. *J. Phys. Chem.* **1994**, *98*, 952–959.
(122) Tachibana, Y.; Moser, J. E.; Grätzel, M.; Klug, D. R.; Durrant, J. R. *J. Phys. Chem.* **1996**, *100*, 20056–20062.
(123) Kelly, C. A.; Farzad, F.; Thompson, D. W.; Stipkala, J. M.; Meyer, G. J. *Langmuir* **1999**, *15*, 7047–7054.
(124) Mulhern, K. R.; Detty, M. R.; Watson, D. F. *J. Phys. Chem. C* **2011**, *115*, 6010–6018.
(125) Nozik, A. J. *Annu. Rev. Phys. Chem.* **1978**, *29*, 189–222.
(126) Hagfeldt, A.; Grätzel, M. *Chem. Rev.* **1995**, *95*, 49–68.
(127) O'Regan, B.; Grätzel, M.; Fitzmaurice, D. *Chem. Phys. Lett.* **1991**, *183*, 89–93.
(128) O'Regan, B.; Grätzel, M.; Fitzmaurice, D. *J. Phys. Chem.* **1991**, *95*, 10525–10528.
(129) Boschloo, G.; Fitzmaurice, D. *J. Phys. Chem. B* **1999**, *103*, 7860–7868.
(130) Benkö, G.; Kallioinen, J.; Korppi-Tommola, J. E. I.; Yartsev, A. P.; Sundström, V. *J. Am. Chem. Soc.* **2002**, *124*, 489–493.
(131) James, D. R.; Liu, Y.-S.; de Mayo, P.; Ware, W. R. *Chem. Phys. Lett.* **1985**, *120*, 460–465.
(132) Gopidas, K. R.; Bohorquez, M.; Kamat, P. V. *J. Phys. Chem.* **1990**, *94*, 6435–6440.
(133) Lakowicz, J. R. *Principles of Fluorescence Spectroscopy*, 2nd ed.; Plenum Press: New York, 1999.
(134) Blackburn, J. L.; Selmarten, D. C.; Nozik, A. J. *J. Phys. Chem. B* **2003**, *107*, 14154–14157.
(135) Farrow, B.; Kamat, P. V. *J. Am. Chem. Soc.* **2009**, *131*, 11124–11131.